Available online at www.sciencedirect.com
ScienceDirect
Ceramics International 37 (2011) 641–645
CERAMICS INTERNATIONAL
www.elsevier.com/locate/ceramint

Microstructure and fracture behavior of β-Si_3N_4 based nanoceramics

Ching-Huan Lee [a], Horng-Hwa Lu [b], Chang-An Wang [c], Wen-Tse Lo [a], Pramoda K. Nayak [a], Jow-Lay Huang [a,*]

[a] Department of Materials Science and Engineering, National Cheng-Kung University, Tainan 701, Taiwan, ROC
[b] Department of Mechanical Engineering, National Chin-Yi University of Technology, Taiping, Taichung 411, Taiwan, ROC
[c] State Key Lab of New Ceramics and Fine Processing, Department of Materials Science and Engineering, Tsinghua University, Beijing 100084, People's Republic of China

Received 30 May 2010; received in revised form 2 September 2010; accepted 4 October 2010
Available online 4 November 2010

Abstract

Fully dense β-Si_3N_4 based nanoceramics were consolidated by spark plasma sintering (SPS). A commercially available β-Si_3N_4 nano-powder was used as starting material. The sintering bulks were fabricated with a heating rate of 90 °C/min by varying SPS temperature from 1550 °C to 1700 °C, and the linear shrinkage was used to evaluate the sintering behavior of the nano-powder. The microstructures of the developed Si_3N_4 based ceramics were achieved, and the grain length, grain width, and aspect ratio for these sintering bulks were found to increase gradually with elevating sintering temperature. The hardness and fracture toughness are associated with the microstructural characteristics. The crack propagation and fracture behavior for these β-Si_3N_4 based nanoceramics have been observed for the specimens sintered at different sintering temperatures. Crack deflection is found to be one of the toughening mechanisms for these β-Si_3N_4 based nanoceramics.

Keywords: B. Microstructure; C. Fracture; Silicon nitride; Nanoceramic; Spark plasma sintering

1. Introduction

Spark plasma sintering technique has provided efficient strategies to activate sintering kinetics for poorly sinterable materials, including nanostructured ones, and results in an overall improvement in materials performance [1]. Among them, Si_3N_4 based ceramics with ultrafined or nanosized grain has shown much potential applications in technical and engineering fields. Only a few studies have demonstrated to fabricate Si_3N_4 based ceramics with finer grain size by SPS. Nishimura et al. [2] got ultrafine-grained Si_3N_4 from finer β-Si_3N_4 powder; Xu et al. [3–5] have fabricated a series of Si_3N_4 based nanoceramics through high-energy mechanical milling and SPS. These finer grained materials are expected to exhibit noticeable high-temperature ductility, improved wear resistance, and elevated hardness [6–9]. However, the use of Si_3N_4 nanoceramics in engineering applications has been limited by the lack of Si_3N_4 nanoprecursor powder and a commercially available sintering process.

Utilization of β-Si_3N_4 based nanopowder prevents the formation of a Si_2N_2O phase, which degrades mechanical, thermal, and tribological properties due to the large agglomeration of nanocrystalline grains and its high temperature instability [10]. Therefore, β-Si_3N_4 nanopowder doped with sintering additives can be used to obtain Si_3N_4 based nanoceramics without complex processing steps, such as high energy milling [3] or carbothermal reduction [9]. In the present study, the β-Si_3N_4 based nanoceramics can be obtained in a proper sintering condition by a large-scale SPS. The aim of this work is to investigate the densification behavior at a fixed heating rate during sintering. The microstructural characteristics and mechanical properties of dense β-Si_3N_4 based nanoceramics were then studied. Owing to the lack of information on the relationship between microstructure and fracture behavior so far, the crack propagation and fracture topography for these nanoceramics with different grain sizes and aspect ratios were discussed in the present study.

* Corresponding author. Tel.: +886 6 2348188; fax: +886 6 2763586.
E-mail address: jlh888@mail.ncku.edu.tw (J.-L. Huang).

0272-8842/$36.00
doi:10.1016/j.ceramint.2010.10.009

2. Experimental procedure

β-Si_3N_4 nano powders (SM131, Fraunhofer-Institut für Keramische Technologien and Sinterwerkstoffe, Dresden, Germany, size 70 nm) doped with sintering additives of 6 wt% Y_2O_3 and 8 wt% Al_2O_3 are taken as the starting material in this present study. The as-received Si_3N_4 powder was first immerged in ethanol and then dispersed by a planetary milling at a rotation speed of 300 rpm for 6 h using a 375 ml Nylon bottle containing Si_3N_4 balls. The slurry was then dried in a rotating vacuum condenser, baked in a vacuum drier, cold-isostatically pressed into round ingots at a pressure of 200 MPa, grinded with mortar and pestle, and screened through a 200-mesh screen to make it to powder form.

The powder was loaded into a graphite mold with an inner diameter of 40 mm. A graphite sheet was inserted into the small gap between the punches and mold, and the graphite mold was also covered with carbon heat insulation. Samples were sintered in a SPS furnace (SPS-3.20MK-IV, Japan) at a mechanical pressure of 50 MPa in vacuum. Samples were sintered at 1550 °C, 1600 °C, 1650 °C, 1700 °C for 4 min with a heating rate of 90 °C/min in vacuum by SPS, and they were designated as B1550, B1600, B1650 and B1700, respectively. Linear shrinkage of the specimens during the SPS process was continuously monitored by displacement of the punch rods. The apparent densities of sintering specimens were measured by Archimedes method. Phase identification was carried out with an X-ray powder diffractometer (XRD; Model D-MAX/II B, Rigaku, Tokyo, Japan). Samples were polished to 1 μm and plasma-etched (95% CF_4 + 5% O_2) for microstructural analysis using SEM (Hitachi S4800-I, Japan). To characterize the grain morphology of sintered Si_3N_4 quantitatively, the grain length and area of each developed grain were measured for over 600 grains with the image analyzer using software (Sigmascan Pro 5.0, SPSS Inc.) and calculated following the statistical derivation by Woetting et al. [11]. The hardness was measured by a Vickers hardness tester (AKASHI AVK-A, Japan) at 196 N for 15 s on

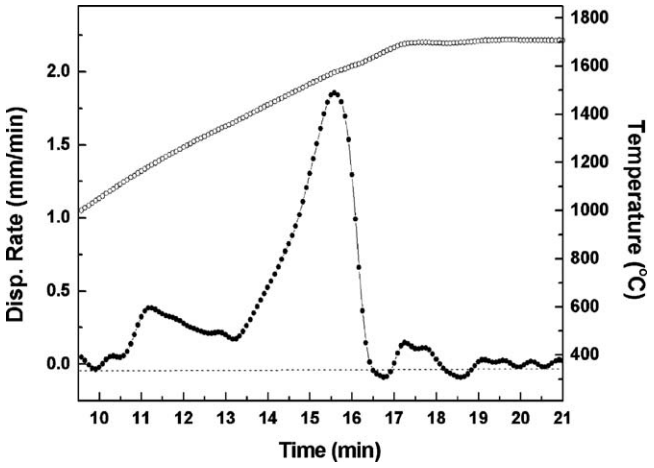

Fig. 1. *In situ* displacement curves for the sintering compacts during the rise of temperature in SPS. The heating rate was controlled at 90 °C/min up to 1700 °C under a uniaxial pressure of 50 MPa in vacuum.

Table 1
Specimen designations and physical properties of specimen.

Designation	Density (g/cm^3)	β-Phase unit cell	
		a_0 (Å)	c_0 (Å)
B1550	3.25	7.619	2.919
B1600	3.25	7.619	2.920
B1650	3.25	7.620	2.921
B1700	3.25	7.621	2.919

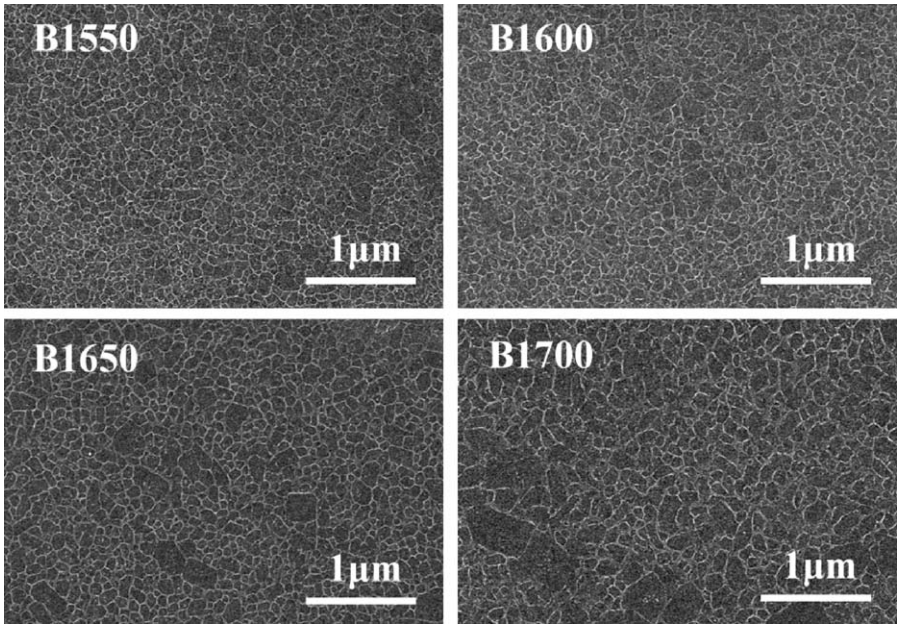

Fig. 2. Typical SEM micrograph for as-sintered Si_3N_4 nano powder; specimen was sintered at 1550 °C, 1600 °C, 1650 °C, 1700 °C for 4 min with a heating rate of 90 °C/min in vacuum by SPS.

polished surfaces. Fracture toughness was determined by the indentation fracture method [12]. Each data point for mechanical properties was measured for at least 5 times.

3. Results and discussion

The displacement of specimens during the SPS process was monitored by that of the punch rods. The densification of specimens was evaluated by the shrinkage rate (dz/dT) calculated from the displacement of the punch rods (z) at a certain temperature (T). Fig. 1 shows the *in situ* shrinkage rate of as-sintered nanosized β-Si_3N_4 powder at temperatures up to 1700 °C. The specimen began to shrink at 1050 °C and completed at 1620 °C. In the temperature interval of 1050–1620 °C, two shrinkage peaks can be seen at 1177 °C and 1573 °C. The results imply that two densification mechanisms take place during the heat-up process. The sintering aids ($Y_2O_3 + Al_2O_3$) may transform from amorphous phase to crystallized one ($3Y_2O_3{\cdot}5Al_2O_3$ or $2Y_2O_3{\cdot}Al_2O_3$) near 1000 °C [13]. Therefore, the occurrence of volume change was due to the phase transformation of sintering aids in the first shrinkage stage. In the second densification stage, the liquid phase formed, leading to the fast consolidation of the sintering compact [14].

The apparent density for each specimen is shown in Table 1. The value of 3.25 g/cm^3 for the apparent density of as-sintered materials was assumed to be near full densification, because no obvious pores were observed on these polished surfaces of sintering bulks. The lattice parameters calculated from X-ray diffraction patterns are shown in Table 1 as well. The value for a_0 and c_0 for β-phase unit cell is ∼7.62 Å and ∼2.92 Å, respectively, which is somewhat deviated from the pure β-Si_3N_4. This result suggests that a β-SiAlON phase might have formed, which is similar with our previous study [14].

Fig. 2 shows the typical microstructure for each specimen sintered at various temperatures for 4 min in vacuum by SPS. No significant elongated grains are observed in these final microstructures. Hence, β-SiAlON with lower aspect ratio was achieved in the SPS process. The frequency distributions of grain length, grain diameter, and aspect ratio of β-SiAlON grains for each specimen, as shown in Fig. 3, were evaluated by image analysis. The results reveal that the grain length, grain width and aspect ratio of specimens B1550, B1600 and B1650 at maximum frequency were similar; whereas these characteristics for the specimen B1700 were slightly greater than the others. The results of image analysis for β-Si_3N_4 based nanoceramics, sintered at different temperatures in vacuum by SPS, are calculated and summarized in Table 2. The ''true'' aspect ratio was obtained from the frequency distribution of the aspect ratio and selecting the value as a_{95}. The average grain length, average grain width and true aspect ratio gradually increase with elevating temperature. Notably, the microstruc-

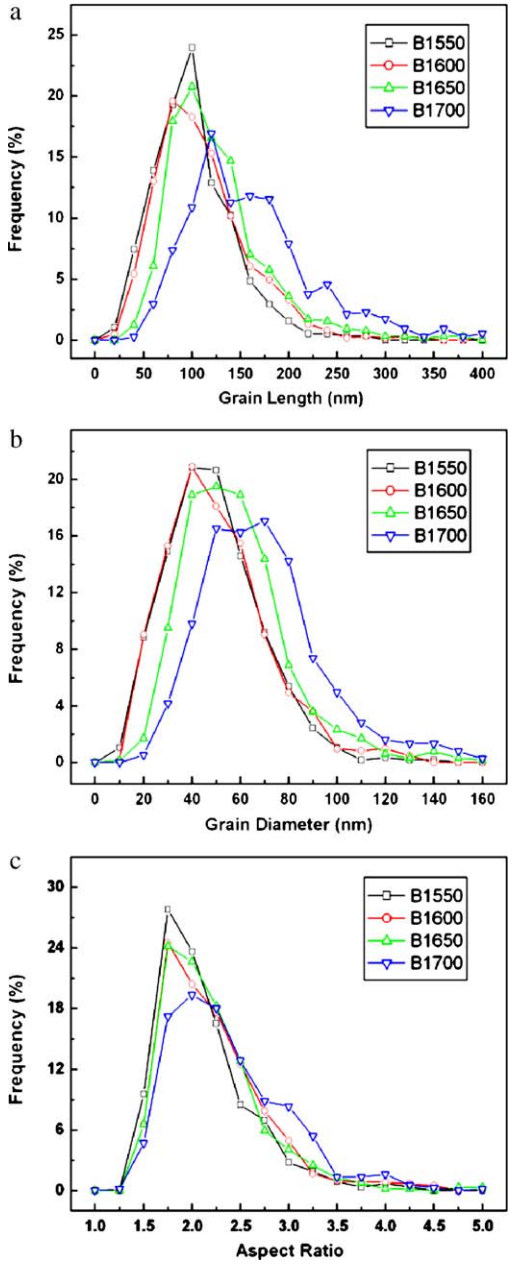

Fig. 3. Frequency distribution of (a) grain length, (b) grain diameter, and (c) aspect ratio of β-SiAlON grains at different sintering conditions.

Table 2
Characteristics of grains for β-Si_3N_4 based nanoceramics sintered at different temperatures.

Designation	Average grain length (nm)	Average grain diameter (nm)	Aspect ratio (a_{95})
B1550	101.7	49.2	3.04
B1600	110.6	50.9	3.18
B1650	125.7	58.6	3.19
B1700	164.5	70.2	3.36

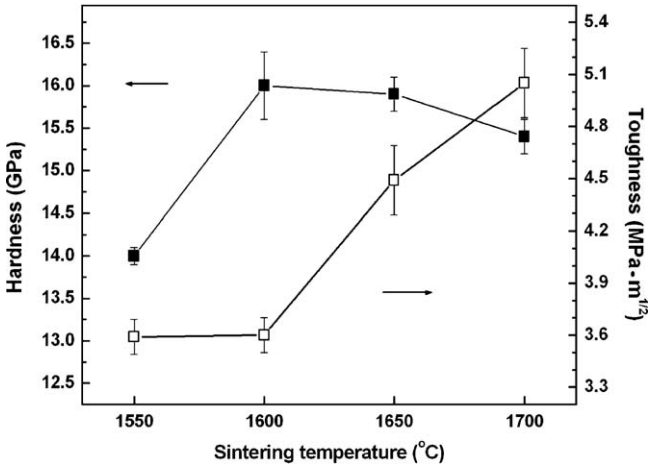

Fig. 4. Hardness and fracture toughness measured by Vickers surface indentation technique as a function of sintering temperature; samples were sintered at 1600 °C for 3 min with a heating rate of 200 °C/min in a vacuum.

tural characteristics for these sintered bulks were found to increase gradually with rising temperature, and the highest value of grain length, grain width, and aspect ratio were achieved in the specimen B1700.

The changes of hardness and toughness are plotted in Fig. 4. A tendency of decrease in hardness and increase in toughness with sintering temperature was noticed. The observed changes in hardness and toughness probably depend on microstructural characteristics, i.e. larger Si_3N_4 based grains have been previously reported to have greater toughness and smaller hardness in Si_3N_4 based grains [9].

To identify the fracture characteristics of these Si_3N_4 based nanoceramics, crack propagation and fracture surface were observed in the present study. The crack ends of the specimen B1600 and B1700, made by micro-indentation, are shown in Fig. 5(a) and (b), respectively. Very similar crack propagation for the two specimens has been observed. This implies that the predominately fracture toughness mechanism is the same for the two specimens with different grain sizes. In general, the debonding path usually occurs at the interface between the grains and intergranular film [15,16]. Hence, the cracks were deflected along the weak grain boundary in the present study. Moreover, the crack bifurcation around grains was frequently observed (as shown in Fig. 6) in the specimen B1700. The phenomena also implied that the damage resistance was probably enhanced for specimen B1700 with increasing crack path.

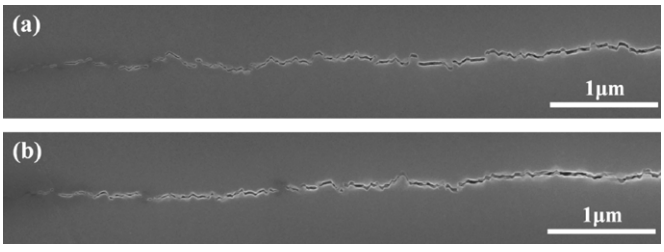

Fig. 5. SEM micrographs showing the crack ends of the specimens (a) B1600 and (b) B1700.

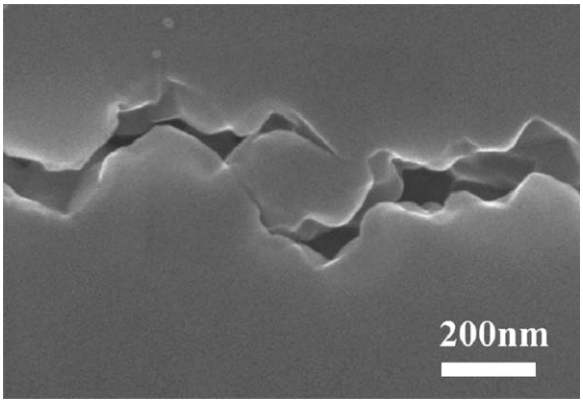

Fig. 6. A typical SEM micrograph showing a crack bifurcation around a larger β-SiAlON grain; the sample was sintered at 1700 °C for 4 min in vacuum by SPS.

The selected fracture surfaces for the specimens B1600 and B1700 were observed by SEM, and the images are shown in Fig. 7(a) and (b), respectively. The specimens have shown different fracture topographies. The fracture surface of specimen B1600 is found to be smooth on the micro-meter scale, whereas a rougher fracture surface can be seen in the specimen B1700. These results implied that the larger β-SiAlON grains in the plane of matrix crack would deflect the crack and cause it to travel around the β-SiAlON grains. Furthermore, rougher fracture topography could be also influenced by other fracture mechanisms, such as grain debonding or pullout [16,17]. Therefore, these factors related to microstructural characteristics of sintering bulk would lead to different fracture behaviors in the present work.

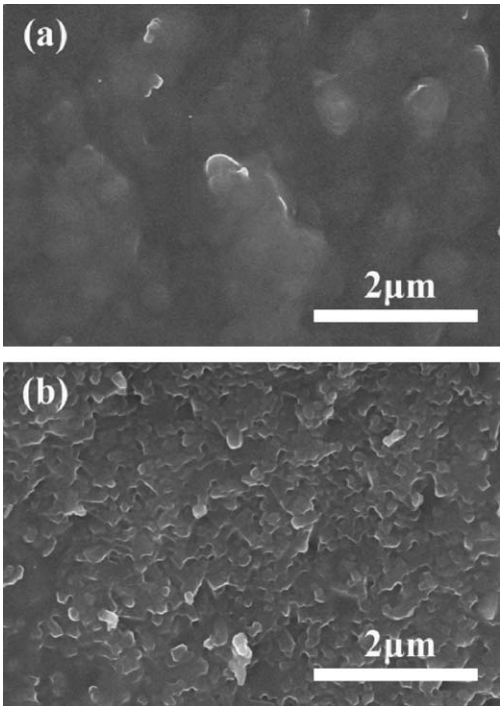

Fig. 7. SEM micrographs showing typical fracture surface of specimen sintered at a sintering temperature of (a) 1600 °C and (b) 1700 °C for 4 min in SPS.

The effect of deflection in the crack propagation path on toughness was investigated by Buljan et al. [18]. An equation showing the increment in toughness as the function of grain size, under the assumption that the grain shapes are same, is given by

$$dK_c = CK_c^0\left(\frac{dD}{D_0} - 1\right) \quad (1)$$

where C is a coefficient dependent on the mode of fracture; K_c^0 and D_0 are the initial toughness and grain size; dK_c and dD are the respective changes in toughness and grain width. The derivation is similar with the observation by Peillon and Thevenot, i.e. toughness is proportional to the grain diameter square root [19]. In addition, Bucevac et al. have exhibited that the β-Si_3N_4 based grains with higher aspect ratio would result in an increase of fracture toughness [20]. As a consequence, both grain width and aspect ratio would affect the fracture toughness. In the present work, the propagating cracks could be deflected by the larger grains (higher grain width and aspect ratio) containing in specimen B1700. In other words, it might decrease the degree of crack deflection due to the existence of nanosized crystallites, leading to a lower damage tolerance for B1600 than that of B1700.

4. Conclusions

Dense β-Si_3N_4 based nanoceramics were fabricated at various temperatures ranging from 1550 °C to 1700 °C by spark plasma sintering. The grain size with a narrow range of average grain length from 101 nm to 165 nm, average grain width from 49 nm to 70 nm, and lower aspect ratio from 3.04 to 3.36 was demonstrated. The grain length, grain width and aspect ratio increase with an increase of sintering temperature. The specimen B1600 exhibits the highest hardness of 16 GPa and the lowest toughness of 3.6 MPa $m^{1/2}$, while the specimen B1700 has a moderate hardness of 15.4 GPa and a highest toughness of 5.05 MPa $m^{1/2}$. Crack deflection was confirmed as one of the toughening mechanisms in these β-Si_3N_4 based nanoceramics. With increasing grain width and aspect ratio of β-Si_3N_4 based grains, both fracture toughness and fracture path tortuosity increase.

Acknowledgment

The authors thank to the National Science Council of the ROC for its financial support under the contract no. NSC 99-2923-E-006-002-MY3.

References

[1] R. Orru, R. Licheri, A.M. Locci, A. Cincotti, G.C. Cao, Consolidation/synthesis of materials by electric current activated/assisted sintering, Mater. Sci. Eng. Rep. 63 (4–6) (2009) 127–287.
[2] T. Nishimura, M. Mitomo, H. Hirotsuru, M. Kawahara, Fabrication of silicon nitride nano-ceramics by spark plasma sintering, J. Mater. Sci. Lett. 14 (15) (1995) 1046–1047.
[3] X. Xu, T. Nishimura, N. Hirosaki, R.J. Xie, Y.C. Zhu, Y. Yamamoto, H. Tanaka, New strategies for preparing nanosized silicon nitride ceramics, J. Am. Ceram. Soc. 88 (4) (2005) 934–937.
[4] X. Xu, T. Nishimura, N. Hirosaki, R.J. Xie, Y. Yamamoto, H. Tanaka, Fabrication of alpha-SiAlON nano-ceramics, in: T. Ohji, T. Sekino, K. Niihara (Eds.), Science of Engineering Ceramics Iii, Key Engineering Materials, vols. 317–318, Trans Tech Publications Ltd., Zurich-Uetikon, 2006, pp. 629–632.
[5] X. Xu, T. Nishimura, N. Hirosaki, R.J. Xie, Y. Yamamoto, H. Tanaka, Fabrication of beta-SiAlON nanoceramics by high-energy mechanical milling and spark plasma sintering, Nanotechnology 16 (9) (2005) 1569–1573.
[6] G.D. Zhan, M. Mitomo, Y. Ikuhara, T. Sakuma, Effects of microstructure on superplastic behavior and deformation mechanisms in beta-silicon nitride ceramics, J. Am. Ceram. Soc. 83 (12) (2000) 3179–3184.
[7] X. Xu, T. Nishimura, N. Hirosaki, R.J. Xie, Y. Yamamoto, H. Tanaka, Superplastic deformation of nano-sized silicon nitride ceramics, Acta Mater. 54 (1) (2006) 255–262.
[8] M. Yoshimura, O. Komura, A. Yamakawa, Microstructure and tribological properties of nano-sized Si_3N_4, Scr. Mater. 44 (8,9) (2001) 1517–1521.
[9] J.H. Kim, B.V.M. Kumar, S.H. Hong, H.D. Kim, Fabrication of silicon nitride nanoceramics and their tribological properties, J. Am. Ceram. Soc. 93 (5) (2010) 1461–1466.
[10] C.P. Dogan, J.A. Hawk, Microstructure and abrasive wear in silicon nitride ceramics, Wear 250 (2001) 256–263.
[11] G. Woetting, B. Kanka, G. Ziegler, Microstructural development, microstructural characterization and relation to mechanical properties of dense silicon nitride, in: S. Hampsire (Ed.), Non-oxide Technical and Engineering Ceramics, Elsevier Applied Science, London, UK, 1986 , pp. 83–96.
[12] A.G. Evans, E.A. Charles, Fracture toughness determination by indentation, J. Am. Ceram. Soc. 59 (7, 8) (1976) 371–372.
[13] A. Bondar, L.N. Kordera, Physicochemical study of yttrium aluminate, in: E.M. Savitskii (Ed.), Tugoplavkie Met., Splavy Soedin. Monokrist Strukt., 1984, 119–125.
[14] C.H. Lee, H.H. Lu, C.A. Wang, P.K. Nayak, J.L. Huang, Effect of heating rate on spark plasma sintering of a nanosized β-Si_3N_4 based powder, J. Am. Ceram. Soc. (submitted for publication) doi:10.1111/j.1551-2916.2010.04196.x.
[15] P.F. Becher, Microstructural design of toughened ceramics, J. Am. Ceram. Soc. 74 (2) (1991) 255–269.
[16] P.F. Becher, G.S. Painter, M.J. Lance, S. Ii, Y. Ikuhara, Direct observations of debonding of reinforcing grains in silicon nitride ceramics sintered with yttria plus alumina additives, J. Am. Ceram. Soc. 88 (5) (2005) 1222–1226.
[17] P.F. Becher, E.Y. Sun, K.P. Plucknett, K.B. Alexander, C.-H. Hsueh, H.-T. Lin, S.B. Waters, C.G. Westmoreland, E.-S. Kang, K. Hirao, M.E. Brito, Microstructural design of silicon nitride with improved fracture toughness: I, effects of grain shape and size, J. Am. Ceram. Soc. 81 (11) (1998) 2821–2830.
[18] S.T. Buljan, J.G. Baldoni, J. Neil, G. Zilberstein, Dispersoid-toughened silicon nitride composites, ORNL/Sub/85-22011/1, GTE, 1988
[19] F.C. Peillon, F. Thevenot, Microstructural designing of silicon nitride related to toughness, J. Eur. Ceram. Soc. 22 (3) (2002) 271–278.
[20] D. Bucevac, S. Boskovic, B. Matovic, L. Zivkovic, M. Vlajic, V. Krstic, Correlation between fracture toughness and microstructure of seeded silicon nitride ceramics, J. Mater. Sci. 42 (18) (2007) 7920–7926.